12th International Conference on Fracture Mechanics of Concrete and Concrete Structures
FraMCoS-12
B.L.A. Pichler, Ch. Hellmich, P. Preinstorfer (Eds)

https://doi.org/10.21012/FC12.1181
MS03-2:3

FRACTURE ASSESSMENT OF SMALL AND LARGE-SCALE STEEL FIBRE REINFORCED CONCRETE SPECIMENS USING ACOUSTIC EMISSION AND DIGITAL IMAGE CORRELATION TECHNIQUES

ROSHINI RAMANATHAN[*] AND KEERTHANA KIRUPAKARAN[†]

[*†] Indian Institute of Technology Madras
Chennai, India
[*]e-mail: roshinicivil14@gmail.com
[†]e-mail: keerthanak@civil.iitm.ac.in

Key words: Steel Fibre Reinforced Concrete, Acoustic Emission, Digital Image Correlation, Fracture mechanics

Abstract: The fracture assessment of concrete and concrete composites using Digital Image Correlation (DIC) and Acoustic Emission (AE) techniques is commonly performed on small-scale laboratory specimens, with findings then extrapolated to large-scale structures. DIC provides detailed surface displacement and macrocrack visualization, while AE offers real-time tracking of micro and macro cracks. However, in real-world scenarios, factors such as structural geometry, variations in loading and background noise can significantly affect AE and DIC data, making interpretation challenging. This study examines small-scale standard notched Steel Fiber Reinforced Concrete (SFRC) beams and large-scale precast SFRC tunnel segments under three-point bending (3PB) to conduct a comparative analysis of fracture behaviour. The influence of tunnel geometry, casting methods, and loading conditions on fracture behaviour is emphasized. The similarities and differences in fracture mechanisms between small-scale beams and large-scale tunnel segments are identified.

1 INTRODUCTION

Steel Fiber Reinforced Concrete (SFRC) has gained significant attention in the construction industry as it enhances the durability of civil structures. The higher toughness of SFRC and its ability to control crack width help resist corrosion, thereby improving the service life of the structure. The fibres in SFRC get activated essentially after the first crack and thereafter softening or hardening behaviour is observed depending upon the volume fraction of fibres. The design of SFRC structural elements is based on fracture mechanics principles. Therefore, accurate determination of fracture parameters is critical for the safe design of SFRC structures. Fracture energy (G_f) and size of the fracture process zone (FPZ) are two important parameters to characterize the fracture behaviour of quasi-brittle materials.

Under load, a significant inelastic zone forms ahead of the crack tip, known as the FPZ, which is governed by complex toughening mechanisms like microcracking, crack deflection, crack branching, aggregate bridging fibre bridging and crack tip blunting by voids [1]. While fracture energy is typically determined experimentally from the load-displacement curve [2], the determination of the FPZ size of concrete is not straightforward. Non-destructive techniques such as digital image correlation (DIC) and acoustic emission (AE) are often used to characterize the FPZ size in concrete. The fracture assessment of SFRC using DIC and AE techniques is usually done on small-scale laboratory specimens with DIC

offering surface displacement and macrocrack visualization and AE tracking micro and macro cracks in real-time. While controlled laboratory conditions allow for effective AE and DIC correlation with the global material response, extrapolating these results to large-scale structures presents significant challenges. In real-world applications, various factors such as structural geometry, load variability, and background noise can significantly influence data acquisition.

The development of a fully formed FPZ in small-sized specimens under bending tests is still in debate. In bending, the top part of the beam is in compression, which restricts the full development of the FPZ. Recent studies show that while tensile tests, can result in a fully developed FPZ for both small and large specimens, this is not observed in small specimens during bending [3]. Previous studies, by Wu et al. [4] using DIC to study the FPZ in plain concrete beams under three-point bending could develop a fully opened FPZ when the Crack Tip Opening Displacement (CTOD) reached a critical value. It was also noted that the FPZ length increases until fully developed and then decreases. Similarly, Alam et al. [5] used DIC to investigate the size effect in crack propagation, finding that smaller beams exhibit relatively longer crack lengths. Saucedo et al. [6], have explored FPZ development in smaller beams and defined the length of the fully developed FPZ as the distance between the crack tip with no cohesive stress and the crack tip where the cohesive stress reaches the material's tensile strength. However, the variation of FPZ along the width of the specimen is assumed to be constant in small-scale specimens as the crack propagation in these specimens is more localized and does not exhibit significant variation across the width. In contrast, the large-scale specimens are modelled using plane strain conditions, assuming that the crack propagation is more distributed across the width due to the specimen's larger dimensions and more complex stress distribution. This simplifies the analysis by considering that the strain in the thickness direction is negligible, where the effect of confinement is less pronounced compared to small specimens. The mesoscale numerical model of SFRC tunnel linings developed by Yang et al. [7] with uniform loading shows that the damage variable distribution of the concrete matrix is uniform across the width. While studies [8] with large-scale testing analyse the mechanical behaviour, the fracture behaviour is still underexplored.

In this study, an attempt has been made to assess the fracture behaviour of small and large-scale SFRC specimens under three-point bending (3PB) using AE and DIC techniques.

2 EXPERIMENTAL PROGRAM

A concrete mix with a characteristic compressive strength of 50 MPa is used in both scale specimens. With 435 kg/m^3 of cement, the ratio of cement, fine and coarse aggregate is 1: 1.6: 2.4. Supplementary cementitious materials (SCMs) were added in the ratio of 1 (Cement): 0.12 (Fly ash): 0.06 (Micro silica). The mix includes 40 kg/m^3 of 4D hooked-ended steel fibres, each 60 mm long and 0.75 mm in diameter and 0.9 kg/m^3 of polypropylene fibres to avoid shrinkage cracks.

The AE sensor locations were determined by the attenuation curve. For DIC the speckles were made using black and white spray paint covering only the mid-part of both the tunnel segment and the beam (either side of the notch).

2.1 Notched beam

Prisms of dimensions $700 \times 150 \times 150$ mm were cast and a notch 25 mm deep and 3 mm was cut across the width of the specimen at mid-span, perpendicular to the casting direction. The notched beam test utilizing 3PB as per EN 14651:2005 (E) [9] and RILEM TC 162-TDF [10] guidelines was adopted. 80 mm on either side of the notch is painted with white spray paint and speckles were done using black spray paint for DIC analysis. For the acoustic emission (AE) a total of 6 sensors were used with 3 on each on the front and back face with the configuration as shown in Figure 1.

Testing is conducted using a 1000 kN MTS servo-hydraulic closed-loop testing system with a 100 kN load cell. For Crack Mouth Opening Displacement (CMOD) measurement,

a clip gauge is affixed to a pair of 3 mm thick knife edges positioned across the notch at the mid-width of the specimen.

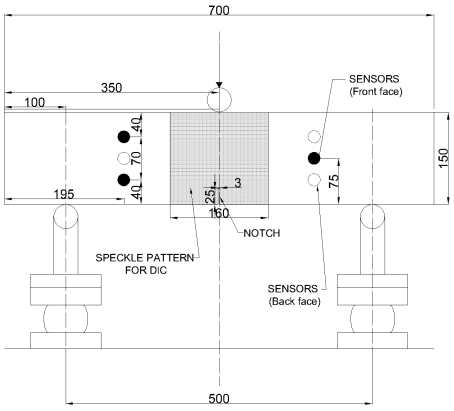

Figure 1: Notched beam test setup

2.2 Tunnel segment

The precast curved tunnel segment of dimensions 3400 × 1400 × 275 mm is shown in Figure 2. The inner radius is 2900 mm and the outer radius is 3175 mm. The segments were cast with the extrados surface facing upwards and were compacted by vibration. The acoustic sensors were placed in a staggered manner, after performing attenuation as shown in Figure 2. With a span of 3000 mm, the 3PB was done with 40 tons capacity flexure machine (Figure 3).

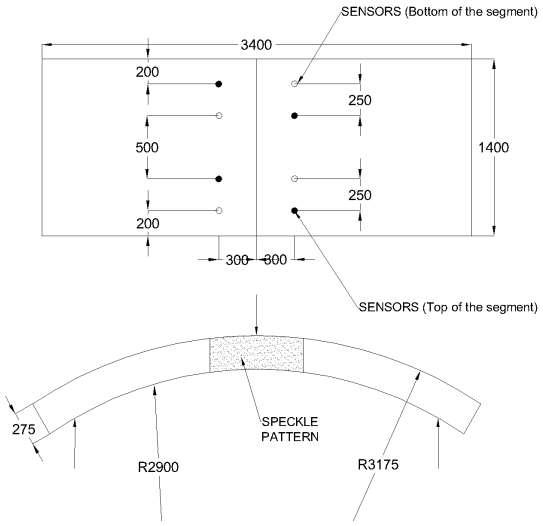

Figure 2: Tunnel segment setup

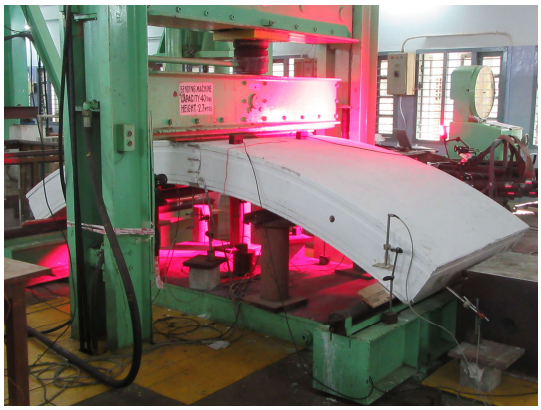

Figure 3: Tunnel segment 3PB setup

3 MECHANICAL BEHAVIOUR

The load-deflection plot of both tunnel and notched beam is shown in Figure 4.

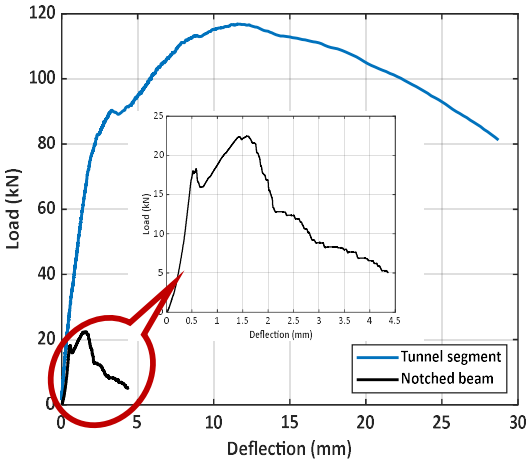

Figure 4: Load-deflection plot of tunnel segment and notched beam

In both cases upto peak load, the concrete matrix experiences elastic deformation, and cracks begin to form when the applied load reaches approximately 80% of its maximum load. Then a fracture failure occurs within the matrix. Simultaneously, the applied load shifts or stress transfer occurs making steel fibres active thereby a strain-hardening region develops. Finally, debonding and bridging occur at the interface between the concrete and the steel fibres, leading to the steel fibres being gradually pulled out from the matrix. The tunnel segment is typically a more massive and

geometrically complex structure, which results in a gradual transition from linear to nonlinear behaviour. This is because the larger size and more distributed load allow the stress to be distributed more evenly across the structure. The notched beam, on the other hand, has a pre-existing crack or notch that serves as a stress concentration point. Under loading, the notch quickly leads to crack propagation, causing a rapid transition from elastic to nonlinear behaviour. This is also reflected in the determination of the Limit of Proportionality, $f_{ct,L}^{f}$ (LOP) [9]. The LOP of the notched beam and tunnel is obtained as 5.78 N/mm^2 and 3.83 N/mm^2. The concentration of stress at the notch causes the material to fail more rapidly after reaching the peak load, which leads to a higher LOP value, as the load is concentrated in a smaller, more critical area. In the tunnel segment, the applied load is spread over a wider region, reducing the maximum stress at any given point. Therefore, the average load per unit width (LOP) in the tunnel segment is lower compared to the notched beam.

4 FRACTURE BEHAVIOUR

4.1 Digital Image Correlation (DIC) analysis

Digital image correlation (DIC) is a non-contact optical method used for measuring displacements across the surface of a target object. It involves capturing images of the surface before and after deformation using a digital camera, from which displacements at specific points are calculated using a correlation algorithm. The photos were captured at a frequency of 5 Hz using the 12.3 MPx camera placed on the tripod support which is positioned parallel to the plane of the specimen.

The tip of the Fracture process zone (FPZ) was quantified by the methodology proposed by Bhowmik and Ray [11]. They proposed a gradient-based method to estimate the size of the fracture process zone (FPZ). This method involves identifying the tip of the FPZ by locating the point where the horizontal displacement gradient becomes negligible. This was done at the peak load step. The length of the fracture process zone for the notched beam and tunnel segment is obtained as 80.43 mm and 183.50 mm respectively. When concrete cracks, it creates localized stress concentrations due to the interruption in material continuity and the redistribution of loads. The adjacent concrete must compensate for the loss of structural integrity, leading to higher strains as it adjusts to the new stress distribution. This is visualized as higher strains around the crack from DIC (Figure 5).

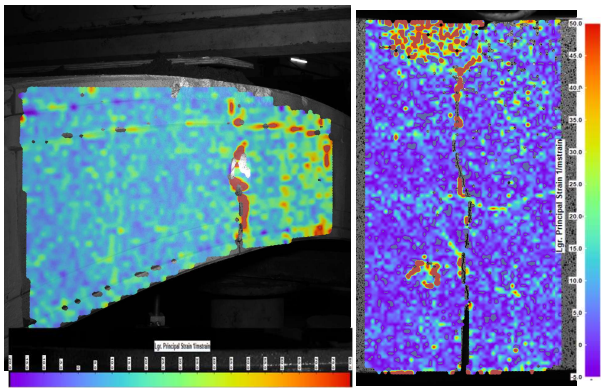

(a) (b)

Figure 5: DIC Lagrangian Strain contour of (a) Tunnel segment (b) Notched beam

4.2 Acoustic Emission (AE) analysis

Acoustic Emission (AE) is a non-destructive testing technique that detects and analyzes the ultrasonic waves emitted by materials undergoing mechanical stress or deformation. Its principle lies in the fact that when materials experience damage, such as crack initiation or propagation, internal stress is rapidly released, generating transient elastic waves. These waves, of a broad frequency spectrum, are captured by sensors, typically piezoelectric transducers and are converted into electrical signals. These signals are then amplified, filtered and analyzed in real-time to provide insights into the nature, location, and severity of the occurring damage. The absolute energy in atto Joules (aJ) from AE events is used to characterize the different levels of damage [12]. The temporal evolution of cumulative energy and load for beam and tunnel specimens are obtained. From Figure 6 it is observed that there is an increase in AE energy only after the first

peak where the load curve drops indicating the first crack and gradually increases in the post-peak region. The simpler geometry of a beam results in more predictable and localized stress distributions. This leads to more distinct damage initiation and propagation events, which are reflected in the step-like AE behaviour. On the other hand, Figure 7 shows an initial smooth increase in AE energy. This is due to the complex geometry, the damage initiation and propagation can be delayed due to stress redistribution. For both specimens, the cumulative AE energy remains constant for a large period in the post-peak of both specimens, which may indicate that the crack growth has stabilized or ceased. The specimen is in a phase where no new cracks are forming or existing cracks are not propagating significantly. This is attributed to the crack-arresting property of the fibres.

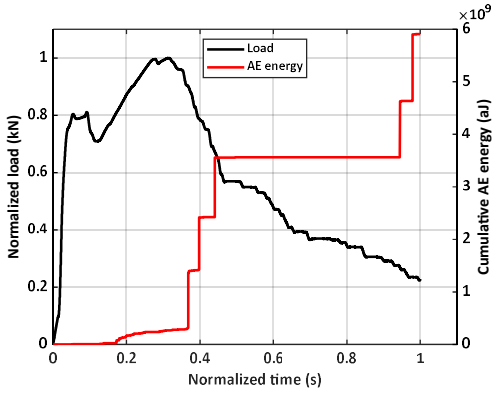

numbersFigure 6: Variation of load and cumulative AE energy with time for the notched beam

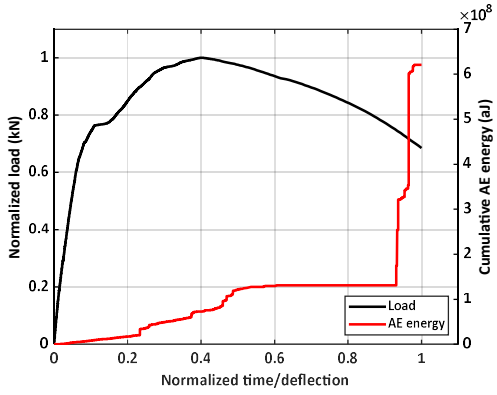

Figure 7: Variation of load and cumulative AE energy with time for the tunnel segment

The AE events were distributed along the specimen dimension. From Figure 8, it was observed that the tunnel segment exhibits a more distributed AE event pattern due to the complex stress distribution and crack propagation. The notched beam exhibits a more localized AE event pattern due to the notch-induced stress singularity and controlled crack propagation.

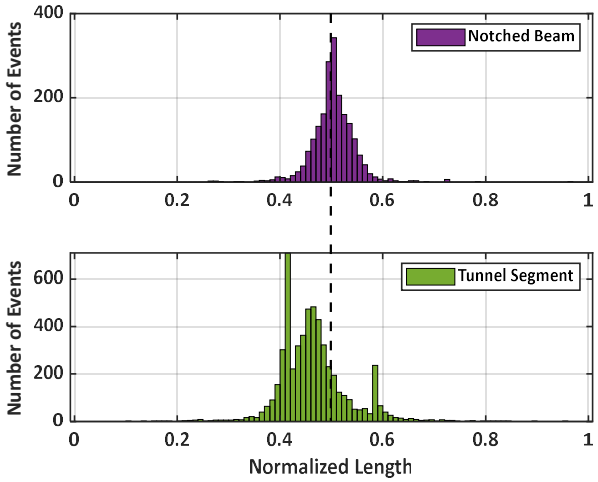

Figure 8: AE event distribution across the length of the specimens

While this distribution remains almost constant for the beam, a variation of FPZ along the width of the tunnel segment was observed (Figure 9). This huge variation can be attributed to several factors, including the non-uniform distribution of fibres, material heterogeneity, and geometrical effects. Fibre segregation may occur as the specimen is cast extrados surface facing upwards. As a result, the end portions of the segment tend to contain a higher concentration of fibres, while the centre section has significantly fewer fibres. Additionally, there could be a variation along the thickness, with the intrados containing more fibres compared to the extrados, suggesting a minor settlement of fibres. The stress distribution along the width of the tunnel segment is not uniform due to loading conditions, geometry and support effects, leading to localized areas of higher or lower stress. These factors collectively contribute to the non-uniform FPZ width along the tunnel segment.

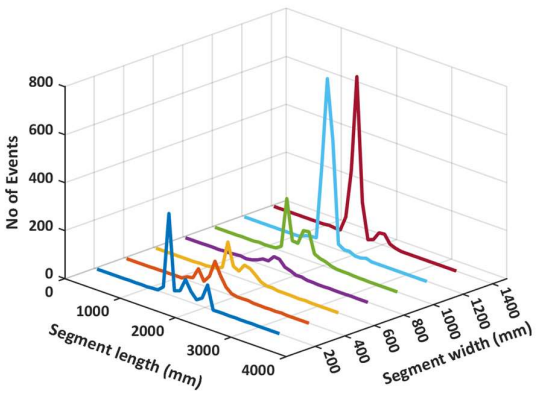

Figure 9: Variation of distribution of AE events along the width of the tunnel segment

5 CONCLUSIONS

This study investigated the fracture behaviour of small-scale and large-scale Steel Fiber Reinforced Concrete (SFRC) specimens using Acoustic Emission (AE) and Digital Image Correlation (DIC) techniques under three-point bending (3PB).

1. From the mechanical behaviour, it was observed that both the specimens exhibited an elastic deformation phase followed by crack initiation and progression once approximately 80% of the maximum load was reached. The strain hardening is due to a higher volume fraction of fibres. The transition to nonlinear behaviour was more rapid in the notched beam, where the pre-existing notch acted as a stress concentrator, compared to the gradual transition observed in the tunnel segment due to its more complex geometry and larger size.

2. The DIC analysis revealed a fracture process zone length of 80.43 mm for the notched beam and 183.50 mm for the tunnel segment, indicating a significantly larger FPZ in the large-scale specimen, which reflects the more distributed stress across the specimen.

3. From AE analysis it was found that the cumulative AE energy for both specimens remained relatively constant in the post-peak region, suggesting stabilization in crack growth or arrest, facilitated by the fibre reinforcement.

The novelty of this study lies in the observed non-uniform variation of the Fracture Process Zone (FPZ) along the width of the specimen, which deviates from conventional plane strain assumptions. Typically, FPZ width is considered to be larger at the surface, decreasing uniformly towards the mid-width, and then increasing symmetrically at the opposite surface. However, the analysis reveals that FPZ evolution is significantly influenced by factors such as non-uniform loading distribution, fiber segregation, and localized variations in material heterogeneity. These effects contribute to an asymmetric and irregular FPZ distribution, which must be accounted for in numerical and analytical modelling approaches to ensure accurate fracture predictions in SFRC structures.

ACKNOWLEDGEMENTS

The authors gratefully acknowledge the support provided by the SRG/2023/002398 grant from the Department of Science and Technology – SERB, Government of India. They also express their appreciation for the FIST Grant SR/FST/ETII-054/2012, which facilitated the acquisition of equipment for the Mechanical Performance of Civil Engineering Materials laboratory at IIT Madras, Chennai, India. The authors thank the support of Larsen and Toubro Limited, Heavy Civil Infrastructure for providing the tunnel segment produced at their casting facility. Additionally, the authors extend their thanks to the Centre of Excellence on Technologies for Low-Carbon and Lean Construction at IIT Madras for their valuable support.

REFERENCES

[1] Kumar, Prashant. *Elements of fracture mechanics*. McGraw-Hill Education LLC., 2009.

[2] RILEM committee on fracture mechanics of concrete, Determination of the fracture energy of mortar and concrete by means of three-point bend tests on notched beams, Materials and structures 18 (106) (1985) 285 290.

[3] Boukais, A., Dahou, Z. and Matallah, M.,

2023. Maximum aggregate size effects on the evolution of the FPZ and crack extensions in concrete–Experimental and numerical investigation. *International Journal of Solids and Structures*, *269*, p.112181.

[4] Wu, Z., Rong, H., Zheng, J., Xu, F. and Dong, W., 2011. An experimental investigation on the FPZ properties in concrete using digital image correlation technique. *Engineering Fracture Mechanics*, *78*(17), pp.2978-2990.

[5] Alam, S.Y., Loukili, A. and Grondin, F., 2012. Monitoring size effect on crack opening in concrete by digital image correlation. *European journal of environmental and civil engineering*, *16*(7), pp.818-836.

[6] Saucedo, L., Yu, R.C. and Ruiz, G., 2012. Fully-developed FPZ length in quasi-brittle materials. *International journal of fracture*, *178*, pp.97-112.

[7] Yang, K., Yan, Q. and Zhang, C., 2021. Three-dimensional mesoscale numerical study on the mechanical behaviors of SFRC tunnel lining segments. *Tunnelling and Underground Space Technology*, *113*, p.103982.

[8] Nehdi, M.L., Abbas, S. and Soliman, A.M., 2015. Exploratory study of ultra-high performance fiber reinforced concrete tunnel lining segments with varying steel fiber lengths and dosages. *Engineering Structures*, *101*, pp.733-742.

[9] Test Method for Metallic Fibered Concrete (2005) Measuring the Flexural Tensile Strength (Limit of Proportionality (LOP), Residual), EN 14651, CEN, Brussels.

[10] RILEM TC 162-TDF Test and Design Methods for Steel Fibre Reinforced Concrete – Final Recommendations, Materials and Structures, 2002, Vol. 35, pp. 579-582.

[11] Bhowmik, S. and Ray, S., 2019. An experimental approach for characterization of fracture process zone in concrete. *Engineering Fracture Mechanics*, *211*, pp.401-419.

[12] Keerthana, K. and Kishen, J.C., 2020. Micromechanics of fracture and failure in concrete under monotonic and fatigue loadings. *Mechanics of materials*, *148*, p.103490.